Measurements of Elastic Electron-Deuteron Scattering at High Momentum Transfers*

J. E. Elias, J. I. Friedman, G. C. Hartmann, H. W. Kendall, P. N. Kirk, M. R. Sogard, and L. P. Van Speybroeck†

Department of Physics and Laboratory for Nuclear Science, Massachusetts Institute of Technology, Cambridge, Massachusetts 02139

AND

J. K. de Pagter‡

Cambridge Electron Accelerator, Cambridge, Massachusetts 02138

(Received 2 July 1968)

Measurements of cross sections for elastic electron-deuteron scattering were made over a range of four-momentum transfers squared from 14.4 to 35.4 F^{-2}. Incident electrons of energies 4.419 and 4.910 BeV were scattered from a liquid-deuterium target and detected in coincidence with the recoil deuterons. Measurements of a combination of the charge and electric quadrupole moment form factors were obtained from the cross sections, and detailed comparisons were made with theoretical predictions based on wave functions derived from nucleon-nucleon scattering experiments. Good agreement was found with a few of the wave functions used. Theoretical estimates of meson-exchange-current enhancements and relativistic effects were also compared to the data.

I. INTRODUCTION

THE experimental study of the electromagnetic properties of the deuteron using high-energy elastic electron scattering has provided information about the short-range spatial structure of the bound neutron-proton system.[1–9] Electron scattering at large momentum transfer probes the short-distance structure of the n-p wave function, which can in turn be related to the short-distance behavior of the n-p interaction. Short-distance behavior of the n-p interaction has also been studied in nucleon-nucleon (N-N) scattering experiments. However, in these latter experiments high momentum transfers are attainable only when the relative energy in the N-N center-of-mass system is large. In electron-deuteron scattering the N-N center-of-mass energy is independent of the electron's momentum transfer. Thus electron scattering can be programmed so that the n-p center-of-mass energy is kept constant while the momentum transfer relevant to probing the n-p structure is varied. In particular, elastic e-d scattering probes the n-p system when the n-p center-of-mass energy is fixed at -2.2 MeV. Inelastic e-d scattering can be programmed to hold the n-p center-of-mass energy in the final state at any desired value as the momentum transfer is varied. Both types of experiment can provide an answer to the question of whether the short-range spatial dependence of the n-p interaction predicted from N-N scattering at large center-of-mass energies is also valid at low center-of-mass energies, a question on which direct experimental evidence from N-N scattering sheds little light.

The present experiment has measured the elastic e-d scattering cross section over a range of the square of the four-momentum transfer, q^2, from 14.4 to 35.4 F^{-2}, where $q^2=4EE'\sin^2(\frac{1}{2}\theta_e)$, E and E' are the energies of the incident and scattered electron, respectively, and θ_e is the electron scattering angle. The highest value of q^2 obtained in earlier measurements[7] was 20 F^{-2}. The present experiment was carried out at electron scattering angles of about 10°, and the measurements are therefore sensitive primarily to the structures of the charge and electric quadrupole moment distributions of the deuteron. The theoretical predictions of the contributions of both the charge and magnetic moment distributions to the cross section are very much smaller than that of the electric quadrupole moment distribution in the range of q^2 from about 15 to 25 F^{-2}. This enables effects of the quadrupole moment distribution to be isolated in this range of q^2. At values of q^2 greater than about 20 F^{-2}, relativistic corrections and possible meson exchange contributions are expected to become important. The present measurements provide data to compare with the theoretical predictions of these

* This work is supported in part through funds provided by the Atomic Energy Commission under Contract No. AT(30-1)-2098. Parts of this work are based on dissertations for the Ph.D. degree submitted to the Department of Physics, Massachusetts Institute of Technology, by G. C. H. and L. P. V.

† Now at American Science and Engineering, Cambridge, Mass.

‡ Now at Southern Massachusetts Technological Institute, North Dartmouth, Mass.

[1] J. A. McIntyre and S. Dhar, Phys. Rev. **106**, 1074 (1957).

[2] J. I. Friedman, H. W. Kendall, and P. A. M. Gram, Phys. Rev. **120**, 992 (1960).

[3] D. J. Drickey and L. N. Hand, Phys. Rev. Letters **9**, 521 (1962).

[4] D. Benaksas, D. Drickey, and D. Frèrejacque, Phys. Rev. **148**, 1327 (1966); Phys. Rev. Letters **13**, 353 (1964).

[5] B. Grossetête, D. Drickey, and P. Lehmann, Phys. Rev. **141**, 1425 (1966).

[6] E. F. Erickson, *Nucleon Structure*, edited by R. Hofstadter and L. I. Schiff (Stanford University Press, Stanford, Calif., 1963), p. 370; E. F. Erickson, Ph.D. thesis, Stanford Univeristy, 1964 (unpublished).

[7] C. D. Buchanan and M. R. Yearian, Phys. Rev. Letters **15**, 303 (1965); C. D. Buchanan, Ph.D. thesis, Stanford University 1966 (unpublished).

[8] J. Goldemberg and C. Schaerf, Phys. Rev. Letters **12**, 298 (1964).

[9] R. E. Rand, R. F. Frosch, C. E. Littig, and M. R. Yearian, Phys. Rev. Letters **18**, 469 (1967).

effects. The experimental apparatus is described in Sec. II of this paper, and the method of data reduction is described in Sec. III. Section IV summarizes the theoretical predictions of the cross section. In Sec. V, the experimental results of this and other experiments are compared with theory using various deuteron wave functions. Section VI contains a summary and conclusions.

II. EXPERIMENT AND APPARATUS

A. Plan of the Experiment

The experiment was carried out at the Cambridge Electron Accelerator[10] (CEA) and used electron beams of energies of 4.419 and 4.910 BeV. The experimental apparatus was designed to measure elastic *e-d* scattering events by detecting recoil deuterons with the use of a quadrupole magnet spectrometer for momentum analysis, scintillation counter arrays for ionization and range measurements, and a wire spark chamber for determining the momenta of the deuterons. In addition, the scattered electrons were detected in coincidence by a lead-Lucite shower counter which had a solid angle much larger than that of the deuteron detection apparatus. We did not attempt to separate elastic from inelastic events by electron momentum analysis because of the stringent momentum resolution requirement.

The apparatus, illustrated in Fig. 1, was situated at an internal electron beam scattering site of the CEA. The momentum of the recoil particles was analyzed with the use of a quadrupole magnet mounted on a spectrometer carriage. The spectrometer could be set at angles between 30° and 90°. The magnet had an angular acceptance of about 2°, a useful solid angle of about 4 msr, and focused particles of the same momentum along a line lying in the horizontal focal plane. Recoiling deuterons were expected to be accompanied by a large background of protons arising from the photo- and electro-disintegration of deuterons. The detection apparatus was designed to separate protons from deuterons of the same momentum by measuring with scintillation counters the specific ionization of the recoil particles. The specific ionization for deuterons was expected to be about twice as large as for protons. Three ionization measurements were made on each recoiling particle with the use of the counter arrays illustrated in Fig. 1. The arrays were also used to require that particle trajectories cross the appropriate region of the focal plane of the magnet. Because the elastic *e-d* scattering cross section was expected to vary rapidly with angle, the 2° angular acceptance of the magnet was subdivided into approximately 0.3° intervals using the counters of the T array.

It was necessary to measure the momenta of the deuterons with sufficient accuracy to separate elastically scattered deuterons from deuterons associated with coherent pion production. The threshold for this process is about 2% below the momentum of elastic events.

A scintillation-counter array placed in the focal plane of the magnet to measure the momentum of the particles with the required resolution would have caused an unacceptable amount of multiple scattering and energy loss. For this reason, a wire spark chamber consisting of a single plane of wires was employed. The chamber was operated in a mode such that sparks developed between adjacent wires rather than to a ground plane. The chamber spanned an 8% momentum interval. The signals from the chamber were sorted into 16 channels. The counter arrays and spark chamber were rotated for each run so that the wires of the chamber were aligned with the focal line corresponding to the kinematics of elastic scattering.

The ratio of protons to deuterons in the 8% momentum interval exceeded 500 to 1 at the highest measured momentum transfers. In addition, there was a large background of slow protons with specific ionization equal to that of recoil deuterons. The slow protons, originating from the pole faces of the magnet, were separated from deuterons by means of a range requirement. An absorber stopped the slow protons but did not stop the deuterons. The emerging deuterons were detected with a final scintillation counter.

The elastically scattered electrons were detected by a shower counter which had a solid angle about five times larger than that subtended by the deuteron detector. Comparisons of measurements of elastic *e-p* scattering with and without the use of this counter were employed to measure its efficiency.

B. Beam and Target

This experiment utilized a target in the synchrotron vacuum chamber. Electrons were allowed to interact with the target, located about 0.8 in. inside the equilibrium orbit of the accelerator, by decreasing the rf accelerating power at the end of the acceleration cycle. The electrons then drifted radially inward from their equilibrium orbit into the target. Estimates indicate that an electron passed through the target approximately ten times before it was lost from the circulating beam. The spill times ranged from 300 to 800 μsec. The uncertainty in the equilibrium orbit energy was about 0.2%.[11] The energy of electrons that passed through the target was estimated to be about 1.8% lower than that of electrons in the equilibrium orbit. This was calculated on the basis of the properties of the magnetic fields of the CEA machine magnets. We estimate an absolute uncertainty in the energy of $\pm 0.5\%$. The spread in energy resulting from the combined effects of the spill and the width of the target was about $\pm 0.4\%$. This spread contributed to the width of the momentum resolution function. The vertical size

[10] A general description of the accelerator is given by W. A. Shurcliff, Cambridge Electron Accelerator Laboratory (CEAL) Report 1000, 1964 (unpublished).

[11] H. Winick, CEAL Report 1015, 1965 (unpublished).

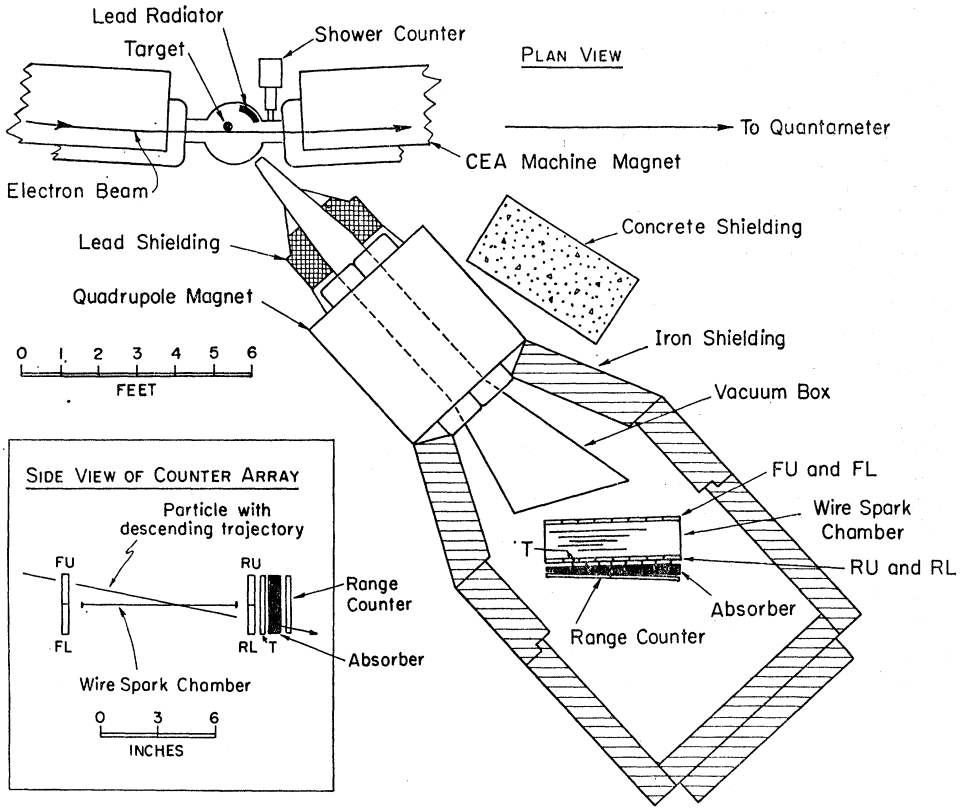

FIG. 1. Experimental site. The positions of the target, deuteron detection system, and the electron shower counter are illustrated. The inset shows a vertical section through the deuteron detection system. A fivefold coincidence of the *FU* or *FL*, *RU* or *RL*, and *T* counters, the range counter, and the shower counter, which satisfied pulse-height requirements and signified an ascending or descending trajectory through the deuteron detection system, caused the spark chamber to be pulsed.

and inward radial drift of the beam was limited by a 0.125-in. collimating slit which shadowed the target. The slit was located on the opposite side of the accelerator from the scattering site in order to avoid background arising from the collimation. The slit could be moved radially to expose different parts of the target to the beam. The target liquid was contained in a 0.5-in.-diam vertical cylindrical vessel made of 0.0005-in. Kapton film. Liquification of the target gases was carried out using cold gaseous helium. A solid target of Kapton, about 0.032 in. thick, was used for calibration and detector efficiency studies.

The product of the target thickness and the incident electron flux was measured by monitoring the bremsstrahlung produced by the interaction of the electron beam with the target. A quantameter[12] filled with a 10% helium and 90% nitrogen gas mixture was used as the monitor. The calibration constant was $U_q = 2.695 \times 10^{19}$ MeV/C. We have assigned an uncertainty of 3.0% to the calibration constant to account for a possible calibration error.[13]

[12] J. de Pagter and M. Fotino, CEAL Report 1022, 1965 (unpublished). CEA quantameter Q1F was used in this experiment.

[13] The intercalibration of CEA quantameters with quantameters, from Cornell University and a Faraday cup from Stanford University is discussed by K. W. Chen, J. R. Dunning, Jr., A. A. Cone, N. F. Ramsey, J. K. Walker, and Richard Wilson, Phys. Rev. **141**, 1267 (1966).

C. Spectrometer, Counters, and Spark Chamber

The spectrometer magnet was a quadrupole with a 12-in.-diam aperture. The magnet was positioned midway in the 174-in. space between the target and the spark chamber. The center of the magnet was blocked by a lead plug to prevent particles from passing through the region of weakest field.

The five scintillation-counter arrays, shown in Fig. 1, used to measure specific ionization, scattering angle, and to determine appropriate trajectories in the spectrometer, were assemblies of plastic scintillator viewed through plastic light pipes by RCA 6342A phototubes. The light collection uniformity varied by about 5% over the area of each counter.

The wire plane of the spark chamber consisted of 64 wires which were 0.01 in. in diameter, 42 in. long, and 0.250 in. apart. Alternate wires were pulsed with a 1500-V pulse and a spark developed between a pulsed wire and an adjacent one along the path of a particle that had traversed the chamber. Signals were derived from 32 signal wires, each grounded through a resistor. Signals from pairs of these wires were added to form 16 channels of information, then passed through discriminators, sorting logic, and into a pulse-height-analyzer core memory for storage. The sorting logic rejected spark patterns involving more than three adjacent bins, and made other decisions regarding acceptable and nonacceptable events.

The range counter following the absorber was constructed from two pieces of scintillation plastic, each viewed by two RCA 6342A phototubes. The thickness of the absorber was tapered to match the variation in deuteron momentum across the angular acceptance of the system. The thickness was adjusted during the experiment to achieve simultaneously high efficiencies for detecting deuterons and for rejecting protons.

The electron shower counter, located 11 in. from the target with one edge 2 in. from the circulating beam of the synchrotron, operated in an environment having a very large flux of background particles. The background originated primarily from electrons interacting with accelerator structure upstream of the target. The counter consisted of a lead block five radiation lengths thick followed by a Lucite Čerenkov counter. The counting rate was constantly monitored and the gain adjusted so that the instantaneous singles rate never exceeded 1 MHz. A 4-BeV electron passing through the counter's lead radiator was expected to produce a shower of about 20 electrons. We replaced the counter at intervals because the Lucite plastic became somewhat darkened by radiation after extended exposure. Small drifts in gain were noted and corrected during the runs.

D. Electronics

A simplified diagram of the electronics logic is shown in Fig. 2. Differential discriminators imposed pulse-height requirements on the pulses from the *FU*, *FL*, *RU*, *RL*, and *T* counter arrays to separate deuterons from protons and other background particles. A pulse routing system, not shown in Fig. 2, permitted several pulse-height spectra to be stored simultaneously. This system allowed continuous checks to be made on the pulse heights selected by the discriminators. The spark chamber was triggered if an event satisfied the pulse-height and range criteria and was associated with a fourfold coincidence between the electron detector and the heavy particle arrays establishing a proper trajectory, *FL*, *RU*, and *T* or *FU*, *RL*, and *T*. Events accepted by the spark chamber sorting logic were stored in one of 112 channels of memory of a pulse-height analyzer (PHA) corresponding to the elements of the matrix determined by the 16 momentum and 7 angle channels.

III. REDUCTION OF EXPERIMENTAL DATA TO CROSS SECTIONS

A. Summary of the Method

The experimental cross sections were obtained by fitting at each angle the sum of a resolution function and a background function to the measured momentum distributions with the method of least squares. Prior to the fitting, corrections were made to the spectra for the detection efficiencies, for the solid angle and momentum acceptances of each channel of the spark chamber, and for other detection efficiencies. The result was divided by the product of the incident flux and target density, measured by the quantameter, to obtain cross sections. The shape of the resolution function was determined from peak shapes obtained in elastic *e-p* scattering. The variation of the width of the resolution function with kinematics, resulting primarily from multiple scattering of the recoil particle, was taken into account. The shape of the resolution function included a tail to represent the effects of radiative degradation in the scattering process. The tail was cut off 2.5% below the elastic peak momentum for the evaluation of the area of the peak. The inelastic contributions arising from the coherent electro- and photo-production of π^0 mesons were estimated to be negligible at the momen-

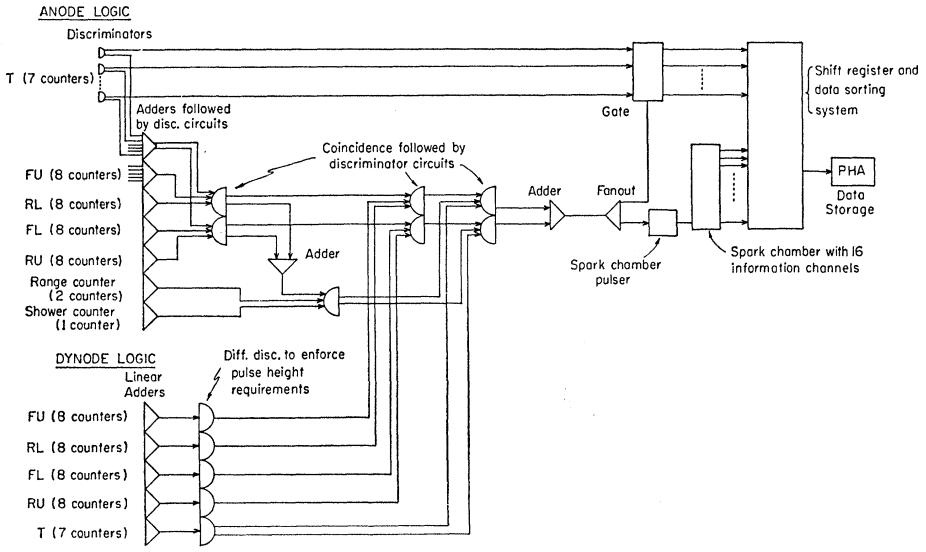

FIG. 2. Simplified electronics logic. The gating system and the pulse-height routing system are not illustrated. Clipped pulses from the anodes of the photomultipliers were employed for fast coincidence measurements. Differential discriminators were employed to impose pulse-height requirements on pulses coming from the last dynode (denoted by dynode).

tum at which the elastic tail was cut off. The calculated radiative correction[14] to this yield was about 4%. The formula used was appropriate for making corrections to an experiment where only the deuteron was detected rather than both the deuteron and the scattered electron detected in coincidence. This procedure was valid because the solid angle and the energy acceptance of the electron detector were sufficiently large.

Explicitly, the cross sections were obtained using the formula

$$\left(\frac{d\sigma}{d\Omega}\right)_{\text{expt}} = \frac{1}{\epsilon_s\epsilon_x\epsilon_D} C_D \frac{1}{1+\delta} \frac{E}{U_q Q}\left(\frac{M_a}{N_A X_0}\right)\frac{1}{1-\beta} A,$$

where ϵ_s, ϵ_x, and ϵ_D are the efficiencies of the shower counter, range counter, and pulse-height identification system, C_D is the dead-time correction for the fast electronics, δ is a radiative correction, E is the energy of the incident electron, U_q is the quantameter calibration constant, M_a is the gram atomic weight of the target liquid, N_A is Avogadro's number, X_0 is the radiation length of the target, β is the fraction of the bremsstrahlung produced by the target wall, Q is the charge collected by the quantameter, and A is the deuteron yield given by

$$A = \int_P^\infty \frac{d^2n}{d\Omega dp} dp.$$

Here P is a momentum 2.5% below the elastic peak momentum and $d^2n/d\Omega dp$ is the resolution function fitted to the data. The normalization and position of $d^2n/d\Omega dp$ were obtained at each angle by fitting[15] the sum of the resolution function and a background function to data which had been corrected for the detection efficiencies and solid angle-momentum acceptances of each bin and for the spark-chamber dead time.

The radiation length of the target comes into the determination of the cross section as a factor $1/X_0$ and indirectly, and weakly, through β. We have used the value $X_0=61.6$ g/cm^2 for hydrogen and assigned an uncertainty of 2% to account for possible corrections to this value.[16]

B. Measurements of Efficiencies and Corrections

1. Solid Angle and Scattering Angle

The solid angle and momentum acceptances of each of the 112 bins of the detector were computed from the properties of the magnet and from the geometry of the counters. The measured values of the fields of a CEA magnet,[17] identical in construction to our magnet, were employed with the SLAC computer program TRANSPORT[18] to compute transfer matrices. The matrices were used with a ray-tracing technique to find the boundaries and acceptances of each bin. The total solid angle was about 4.0 msr. The error in the computation from geometrical uncertainties was estimated to be about 2.0%. The angle of the recoil deuteron or proton was measured with the use of the T-counter array. Each T counter had an acceptance of about 0.3°. The recoil angle was known with an accuracy of about ±0.07°. The estimated uncertainty in the form factor from the uncertainty in the recoil angle is about 2.0%.

2. Spark-Chamber Efficiency

The efficiency of each channel of the spark chamber was measured at the elastic deuteron recoil momentum one or more times each time an elastic e-d point was measured. These measurements used recoil deuterons which were emitted from the solid target when bombarded with electrons. These deuterons, which are copiously produced, were very useful for calibration purposes because of their smooth angular and momentum distributions. The spark-chamber channel efficiencies were obtained from a comparison of the number of acceptable events in the chamber with the number of events measured by the counter arrays. In this comparison corrections were made for the momentum distributions of these deuterons. The deuterons were measured in the neighborhood of each elastic recoil momentum. The measured efficiencies had uncertainties of from 3.0 to 5.0%. The efficiencies were found to depend on the specific ionization of the particles and this was accounted for in the analysis. A spark-chamber dead-time correction was also made. After each spectrum was corrected for the spark-chamber efficiencies and dead time, the sum of the corrected yields was normalized to the number of events measured by the counter arrays. The normalization constant was expected to be unity and was usually this value within its error. Examples of corrected spectra are shown in Fig. 3.

3. Range-Counter Efficiency

The range-counter efficiency was measured just prior to an e-d cross-section measurement using deuterons emitted from the solid target with the same momentum as the elastic deuteron recoil momentum. One of the counter arrays FU, FL, RU, or RL, was pulse-height analyzed, using the range counter as a condition on the

[14] N. Meister and D. R. Yennie, Phys. Rev. **130**, 1210 (1963).

[15] The fitting procedures employed minimized the value of χ^2 by varying parameters with the use of a search technique described by R. A. Arndt and M. H. MacGregor, Phys. Rev. **141**, 873 (1966). The parameters varied in a typical fit were the height and position of the peak, and the height and slope of the background.

[16] J. A. Wheeler and W. E. Lamb, Phys. Rev. **101**, 1836 (1965). Corrections to this result have been discussed in Ref. 13. An experimental measurement using 550-MeV electrons has given the value 63.1±1.8 g/cm^2 [D. Bernstein and W. K. H. Panofsky, Phys. Rev. **102**, 522 (1956)].

[17] P. F. Cooper, Jr., CEA Technical Memorandum 74, 1961 (unpublished); and (private communication).

[18] C. H. Moore, S. K. Howry, and H. S. Butler, Stanford Linear Accelerator Center Report, 1965 (unpublished). We wish to thank Karl Brown of SLAC for assistance in utilizing this program.

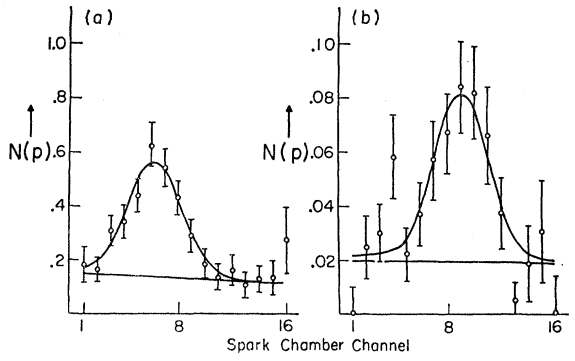

FIG. 3. Examples of deuteron elastic peak data. The momentum spectrum $N(p)$ of the deuteron elastic peak at momentum transfers of 4.0 and 4.75 F^{-1} measured over a single angle bin are shown in arbitrary units, with momentum p denoted by spark-chamber channel number. The data have been corrected for the efficiencies of the spark chamber. The solid lines show fits of the resolution and background functions to the data.

PHA routing. Two spectra were accumulated which showed events that, respectively, triggered and failed to trigger the range counter. The efficiency was obtained from a comparison of the number of events in the two spectra having the pulse-height distribution expected for deuterons. The efficiency varied from about 0.80 to 0.95 with uncertainties of 2.0 to 4.0% over a range of q^2 from 16.0 to 25.0 F^{-2}. At higher values of q^2, a thicker absorber was used to increase proton rejection, and the efficiency dropped to 0.60. The angular dependence of the efficiency was included in the analysis.

4. *Bremsstrahlung from the Target Wall*

The fraction of bremsstrahlung produced by the target wall is given by

$$\beta=\frac{\rho_{\text{wall}}}{X_{0\ \text{wall}}}\int\int I(x,y)L_{\text{wall}}(x,y)dxdy \Big/ \left[\frac{\rho_{\text{wall}}}{X_{0\ \text{wall}}}\int\int I(x,y)L_{\text{wall}}(x,y)dxdy + \frac{\rho_{\text{liq}}}{X_{0\ \text{liq}}}\int\int I(x,y)L_{\text{liq}}(x,y)dxdy\right],$$

where ρ_{wall} and ρ_{liq} are the densities and $X_{0\ \text{wall}}$ and $X_{0\ \text{liq}}$ are the radiation lengths of the target wall and liquid, respectively, $L_{\text{liq}}(x,y)$ and $L_{\text{wall}}(x,y)$ are their respective thicknesses along the beam direction, $I(x,y)$ is a distribution function giving the number of electrons per unit area incident on the target, and x and y are coordinates on a plane perpendicular to the beam. The dependence of $I(x,y)$ on the vertical coordinate y was not important in the determination of β using our own technique since the target thicknesses were independent of y. The dependence on the horizontal coordinate x was determined from measurements of the quantameter yield as a function of the position of the collimator which limited the radial motion of the beam. These measurements were fitted to a sixth-order polynomial with a constraint given by the relationship between $I(x,y)$ and Q,

$$\frac{\rho_{\text{wall}}}{X_{\text{wall}}}\int\int dxdy\, I(x,y)L_{\text{wall}} + \frac{\rho_{\text{liq}}}{X_{\text{liq}}}\int\int I(x,y)L_{\text{liq}}(x,y)dxdy = U_q Q/E,$$

to find the dependence of $I(x,y)$ on x. The fraction β typically had values of 0.11 with uncertainties of 13%. The uncertainty in $(1-\beta)^{-1}$, which enters into the measurements of the cross section, was 1.6%. Most of the uncertainty in β was due to the uncertainty in the determination of $I(x,y)$, and not to uncertainties in the densities and radiation lengths of the target liquid and wall.[19]

5. *Efficiency of the Pulse-Height Selection System*

The efficiency of the *FU*, *FL*, *RU*, *RL*, and *T* counters for identifying deuterons was estimated from studies of the pulse-height spectra of deuterons emitted from the solid target. The efficiency of the system ranged from 0.91 to 0.99 with typical uncertainties of 2.0%.

6. *Fast-Electronics Dead-Time Correction*

A correction for losses arising from the dead time of the fast electronics was estimated for each counter from the singles rates and the dead times of the discriminators and scalers. The correction depended on the beam pulse duration and on the fraction of the accelerator filled with beam. These were constantly monitored. The shower counter had the largest correction. The total correction ranged from 0.5 to 10.0% with typical estimated uncertainties of 0.3%.

7. *Shower-Counter Efficiency*

The efficiency of the electron shower counter was obtained from the ratio of measurments of elastic *e-p* scattering measured with and without this counter required in coincidence. The measurements made with the coincidence not required were compared to other measurements[20] of elastic *e-p* scattering to check the calibration of the equipment. Our measurements, which were in the range of q^2 from 15.2 to 32.5 F^{-2}, were in excellent agreement with these other measurements.

The kinematics of the elastic *e-p* scattering runs were chosen so that the angles of the scattered electrons were the same as those in elastic *e-d* measurements. This

[19] The values of ρ used were: hydrogen 0.0708 g/cm^3, deuterium 0.169, Kapton 1.42. The radiation lengths used were: hydrogen 61.6 g/cm^3, deuterium 123.2, Kapton 41.5.

[20] T. Janssens, R. Hofstadter, E. B. Hughes, and M. T. Yearian, Phys. Rev. 142, 922 (1966).

permitted the efficiency to be measured using an e-p coincidence under conditions similar to those of an e-d measurement. The efficiency was observed to depend on the electron scattering angle, and this effect was included in the analysis. The efficiency typically ranged from 0.70 to 0.95 with uncertainties in each angle bin of about 5.0%.

The momentum spectra obtained from elastic e-p scattering were employed to determine the momentum resolution function. This was approximately Gaussian and the percentage full width at half-maximum for protons varied from (2.20±0.05) to (2.34±0.12)%. The values calculated for protons from the experimental geometry, momentum and angle acceptances, and multiple scattering ranged from 2.12 to 2.20%. The measured widths for deuterons varied from (2.31±0.12) to (2.95±0.12)% and the calculated values ranged from 2.36 to 2.95%.

8. Summary of Uncertainties

The uncertainties in the deuteron elastic peak yields resulting from counting statistics were obtained from the error matrices computed in making least-mean-square fits of the sum of the resolution and background functions to the measured momentum spectra. The elements of the error matrices gave the uncertainties in the parameters describing the fitted functions from which the statistical errors in the cross sections were calculated. These uncertainties were consistent with other estimates based on calculations of the sum of the squares of the differences between the data and the fitted curves (external error) and of the sum of the squares of the statistical errors (internal error). The uncertainties in the channel efficiencies of the spark chamber were added in quadrature to the statistical error prior to the fitting. Other uncertainties are given in Table I. The total uncertainties in the cross-section measurements were the sum of these errors and the statistical errors added in quadrature.

TABLE I. Sources of uncertainty in the measurements other than counting statistics and spark-chamber channel efficiency.

Quantity	Uncertainty (%)
Solid angle	2.0
Heavy-particle recoil angle	2.0
Radiative correction	0.5
Incident electron energy	0.5
Dead-time correction	0.3
Radiation length of hydrogen	2.0
Correction to quantameter yield from target wall bremsstrahlung	1.6
Pulse-height selection efficiency	0.5–2.0
Calibration constant of quantameter	3.0
Range-counter efficiency	2.0–4.0
Shower-counter efficiency	5.0–10.0

TABLE II. The kinematics at which the elastic e-d cross sections were measured.

Incident electron energy (BeV)	Angle of center of spectrometer (degrees)	Range of angles (degrees)	Range of q^2(F^{-2})
4.419	73.00	72.00–73.83	14.4–17.8
4.419	72.00	70.96–72.85	16.2–20.0
4.910	71.50	70.45–72.36	18.2–22.5
4.910	70.49	69.40–71.37	20.4–25.1
4.910	69.50	68.38–70.39	22.7–27.7
4.910	66.50	65.40–67.50	29.7–35.4

9. Experimental Results

The cross sections were measured at two incident electron energies with the spectrometer set at six angles. The kinematics are summarized in Table II. The range counter was not used in the first two sets of runs. Each set consisted of the following measurements: e-p scattering at and 4% above the elastic peak momentum using a hydrogen target, and e-d scattering at the elastic peak momentum and 4% above and below this momentum using a deuterium target. Using the solid target, measurements were made of the efficiencies of the spark chamber, range counter, and pulse-height selection system. The e-p measurements were made both with and without an electron coincidence to measure the efficiency of the electron shower counter. Also, measurements were made with 45-nsec delay inserted in the e-d coincidence circuitry in order to measure the momentum and angular dependence of the chance spectra. Empty target runs could not be made since the target walls were damaged with no liquid in the target. However, empty target runs were simulated using the thicker solid target. The sum of these two backgrounds was consistent with the backgrounds observed as a continuum in the neighborhood of the elastic peak. To avoid the effects of possible normalization errors in the measured background, the background was subtracted by fitting appropriate background shapes to the measured spectra.

The measured values of the cross sections are listed in Table III. These values were divided by the Mott cross section to obtain values of the quantity $A(q^2)+B(q^2)\tan^2(\frac{1}{2}\theta_e)$, defined in the next section. For the kinematics of this experiment, the term $B(q^2)\tan^2(\frac{1}{2}\theta_e)$ was less than 1% of $A(q^2)$ and was neglected in the analysis. Results at different energies and angles, but at essentially the same q^2, were combined using weighted averages to obtain values of $A(q^2)$ listed in Table IV. Figure 4 shows the results of this experiment and values of $A(q^2)$ from other experiments.[1–7]

IV. THEORY

A. General Form of the Elastic *e-d* Cross Section

A number of theoretical calculations have been made of the cross section for elastic *e-d* scattering.[21–27] The calculation used in the analysis of this experiment employed the first Born approximation, the impulse approximation, relativistic kinematics for the electron and recoil deuteron, nonrelativistic deuteron wave functions, and included the electromagnetic structure of the nucleons. Corrections arising from the interaction of the electron with meson currents exchanged between the nucleons[24–26] and from relativistic effects[27] are also included in this analysis.

With the assumptions of the first Born approximation[28] and the relativistic and gauge invariance of the electromagnetic interaction, the cross section for the detection of the recoil deuteron is found to have the following general form:

$$\frac{d\sigma}{d\Omega_d}=\left(\frac{d\sigma}{d\Omega_e}\right)_{\text{Mott}}\left(\frac{d\Omega_e}{d\Omega_d}\right)[A(q^2)+B(q^2)\tan^2(\tfrac{1}{2}\theta_e)],$$

where

$$\left(\frac{d\sigma}{d\Omega_e}\right)_{\text{Mott}}=\frac{e^4}{4E^2}\frac{\cos^2(\frac{1}{2}\theta_e)}{\sin^4(\frac{1}{2}\theta_e)}[1+(2E/M_d)\sin^2(\tfrac{1}{2}\theta_e)]^{-1},$$

and where E is the incident energy of the electron, θ_e is the scattering angle of the electron, $d\Omega_e/d\Omega_d$ is the Jacobian transformation for the solid angle, M_d is the deuteron mass, and e is the charge of the electron.

The quantities $A(q^2)$ and $B(q^2)$ depend on relativistically invariant phenomenological form factors of the deuteron. It has been shown[29] that, with the assumption of time-reversal invariance, a particle of spin one has in general three form factors. In terms of these form factors, the cross section is[27]

$$\frac{d\sigma}{d\Omega_d}=\left(\frac{d\sigma}{d\Omega_e}\right)_{\text{Mott}}\left(\frac{d\Omega_e}{d\Omega_d}\right)\{G_0^2(q^2)+(8/9)\eta^2G_2^2(q^2)+\tfrac{2}{3}\eta G_1^2(q^2)[1+2(1+\eta)\tan^2(\tfrac{1}{2}\theta_e)]\},$$

where $G_0(q^2)$, $G_2(q^2)$, and $G_1(q^2)$ are the charge, quadrupole moment, and magnetic moment form factors, and η is equal to $q^2/4M_d^2$. The explicit angular de-

TABLE III. Values of experimental elastic *e-d* scattering cross sections.

θ_d (deg)	q^2 (F^{-2})	$(d\sigma/d\Omega)_d$ (cm^2/sr)
	Set 1: E=4.419 BeV	
73.83	14.4	$(3.26\pm0.37)\times10^{-34}$
73.59	14.8	$(1.98\pm0.17)\times10^{-34}$
73.25	15.4	$(2.18\pm0.19)\times10^{-34}$
72.92	16.0	$(1.69\pm0.16)\times10^{-34}$
72.60	16.7	$(1.36\pm0.12)\times10^{-34}$
72.29	17.3	$(1.15\pm0.12)\times10^{-34}$
72.00	17.8	$(0.94\pm0.16)\times10^{-34}$
	Set 2: E=4.419 BeV	
72.85	16.2	$(1.37\pm0.27)\times10^{-34}$
72.60	16.7	$(0.88\pm0.16)\times10^{-34}$
72.25	17.3	$(1.05\pm0.15)\times10^{-34}$
71.91	18.0	$(0.75\pm0.11)\times10^{-34}$
71.58	18.7	$(0.70\pm0.15)\times10^{-34}$
71.26	19.4	$(0.72\pm0.14)\times10^{-34}$
70.96	20.0	$(0.79\pm0.13)\times10^{-34}$
	Set 3: E=4.910 BeV	
72.36	18.2	$(8.61\pm1.18)\times10^{-35}$
72.11	18.8	$(5.48\pm0.67)\times10^{-35}$
71.75	19.6	$(6.52\pm0.75)\times10^{-35}$
71.41	20.3	$(4.98\pm0.63)\times10^{-35}$
71.07	21.1	$(4.00\pm0.50)\times10^{-35}$
70.74	21.8	$(2.96\pm0.48)\times10^{-35}$
70.45	22.5	$(2.47\pm0.56)\times10^{-35}$
	Set 4: E=4.910 BeV	
71.37	20.4	$(6.50\pm1.48)\times10^{-35}$
71.10	21.0	$(4.35\pm0.88)\times10^{-35}$
70.74	21.8	$(4.32\pm0.79)\times10^{-35}$
70.39	22.6	$(2.86\pm0.68)\times10^{-35}$
70.04	23.5	$(3.47\pm0.71)\times10^{-35}$
69.70	24.3	$(1.20\pm0.57)\times10^{-35}$
69.40	25.1	$(1.55\pm0.75)\times10^{-35}$
	Set 5: E=4.910 BeV	
70.39	22.7	$(2.60\pm1.15)\times10^{-35}$
70.12	23.3	$(2.36\pm0.68)\times10^{-35}$
69.75	24.2	$(2.67\pm0.71)\times10^{-35}$
69.39	25.1	$(1.86\pm0.63)\times10^{-35}$
69.03	26.0	$(1.38\pm0.62)\times10^{-35}$
68.69	26.9	$(1.60\pm0.68)\times10^{-35}$
68.38	27.7	$(0.67\pm0.41)\times10^{-35}$
	Set 6: E=4.910 BeV	
67.50–66.80	30.91	$(9.74\pm2.68)\times10^{-36}$
66.40–65.40	34.10	$(3.96\pm2.06)\times10^{-36}$

[21] V. Z. Jankus, Phys. Rev. **102**, 1586 (1956).
[22] M. Gourdin, Nuovo Cimento **28**, 533 (1963); **32**, 493(E) (1964).
[23] M. Gourdin, Nuovo Cimento **33**, 1391 (1964).
[24] R. J. Adler and S. D. Drell, Phys. Rev. Letters **13**, 349 (1964).
[25] R. J. Adler, Phys. Rev. **141**, 1499 (1966).
[26] B. M. Casper, Ph.D. thesis, Cornell University, 1966 (unpublished).
[27] F. Gross, Phys. Rev. **142**, 1025 (1966); **152**, 1517(E) (1966).
[28] The first Born approximation has been studied in measurements of e^-p and e^+p scattering to a q^2 of 23.9 F^{-2}. The results are consistent with the approximation. Measurements have been made by R. L. Anderson, B. Borgia, G. L. Cassiday, J. W. DeWire, A. S. Ito, and E. D. Loh, Phys. Rev. Letters **17**, 407 (1966); A. Browman, F. Liu, and C. Schaerf, Phys. Rev. **139B**, 1079 (1965); and D. Yount and J. Pine, Phys. Rev. **128**, 1842 (1962). Recent measurements extend the range to q^2=125 F^{-2}: J. Pine, in *Proceedings of the 1967 International Symposium on Electron and Photon Interactions at High Energies* (Stanford Linear Accelerator Center, Stanford, Calif., 1967), p. 102.
[29] V. Glaser and B. Jaksic, Nuovo Cimento **5**, 1197 (1957); V. M. Dubovik and A. A. Cheshkov, Zh. Eksperim. i Teor. Fiz. **51**, 165 (1966) [English transl.: Soviet Phys.—JETP **24**, 111 (1967)].

pendence permits an experimental separation of the magnetic form factor from the combined charge and quadrupole form factors. Complete separation of the three form factors requires polarization[30] information.

B. Deuteron Form Factors

Expressions for the deuteron form factors have been calculated using relativistic kinematics and nonrelativistic wave functions by a number of authors. Some corrections to the impulse approximation have been considered by Gourdin[31] and have been found to be small compared to the leading terms and also to the meson-exchange corrections and the relativistic corrections, and thus have been neglected in the present analysis. In this theory the nucleons are assumed to have the same form factors as unbound nucleons[32] and nonrelativistic deuteron wave functions are used. The

TABLE IV. Experimental results.[a]

q^2 (F^{-2})	$10^5 A(q^2)$	% error
14.72	42.88±3.69	±8.6
15.42	45.60±4.15	±9.1
16.07	35.75±3.40	±9.5
16.66	28.08±2.53	±9.0
17.29	27.60±2.58	±9.4
18.07	21.66±2.11	±9.7
18.78	15.75±1.79	±11.4
19.52	19.26±2.06	±10.7
20.33	15.88±1.87	±11.8
21.05	13.02±1.48	±11.4
21.82	11.29±1.47	±13.0
22.58	9.33±1.50	±16.1
23.38	10.81±1.87	±17.3
24.25	7.01±1.76	±25.1
25.38	6.75±1.62	±24.0
27.43	4.38±1.67	±38.0
30.90	5.40±1.49	±27.6
34.10	2.57±1.34	±52.1

[a] Values of $A(q^2)$ are derived from the experimental measurements listed in Table III. The errors include both the statistical and systematic errors.

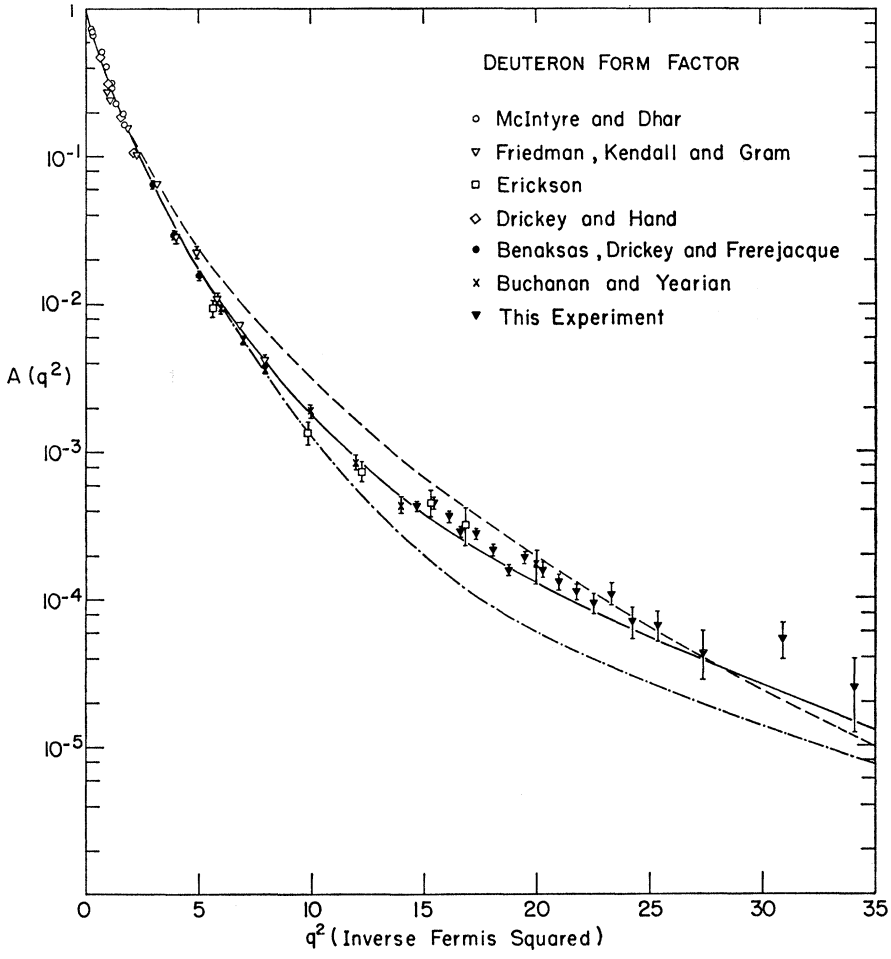

FIG. 4. Measurements of the dimensionless quantity $A(q^2)$. The major contributions to $A(q^2)$ are from the charge and quadrupole moment form factors of the deuteron. The solid, dashed, and dash-dot curves represent the predictions from Hamada-Johnston, Hulthén, and Hulthén hard-core potentials, respectively. The Hulthén hard-core potential has a core at 0.5610 F. The Hulthén predictions are shown to indicate the reliability of simple analytic wave functions.

[30] M. Gourdin and C. A. Piketty, Nuovo Cimento **32**, 1137 (1964).
[31] M. Gourdin, Nuovo Cimento **35**, 1105 (1965).
[32] F. Gross, Ref. 27, has estimated that these effects contribute less than 20% of the relativistic corrections to the cross section.

result of the calculation is[27]

$$G_0=2G_{ES}C_E,$$
$$G_2=2G_{ES}C_Q,$$
$$G_1=2(M_d/M_n)(G_{MS}C_S+\tfrac{1}{2}G_{ES}C_L),$$

where G_{ES} and G_{MS} are the isoscalar electric and magnetic form factors of the nucleon given by

$$G_{ES}=\tfrac{1}{2}(G_{Ep}+G_{En}),\quad G_{MS}=\tfrac{1}{2}(G_{Mp}+G_{Mn}),$$

and

$$C_E=\int_0^\infty [U^2(r)+W^2(r)]j_0(\tfrac{1}{2}qr)dr,$$

$$C_Q=\frac{3}{\sqrt{2}\eta}\int_0^\infty W(r)\left[U(r)-\frac{W(r)}{2\sqrt{2}}\right]j_2(\tfrac{1}{2}qr)dr,$$

$$C_S=\int_0^\infty\left[[U^2(r)-\tfrac{1}{2}W^2(r)]j_0(\tfrac{1}{2}qr)+\frac{W}{\sqrt{2}}\left(U(r)+\frac{W(r)}{\sqrt{2}}\right)j_2(\tfrac{1}{2}qr)\right]dr,$$

$$C_L=\frac{3}{2}\int_0^\infty W^2(r)[j_0(\tfrac{1}{2}qr)+j_2(\tfrac{1}{2}qr)]dr.$$

Here, M_p is the proton mass, $U(r)$ and $W(r)$ are the S- and D-state wave functions of the deuteron normalized so that $\int_0^\infty[U^2(r)+W^2(r)]dr=1$, and $j_0(\frac{1}{2}qr)$ and $j_2(\frac{1}{2}qr)$ are spherical Bessel functions. The static limits of the functions above are:

$$G_0(0)=1,\quad G_2(0)=M_d{}^2Q,$$
$$G_1(0)=(M_d/M_p)[\mu_p+\mu_n-\tfrac{3}{2}P_D(\mu_p+\mu_n-\tfrac{1}{2})],$$
$$G_{ES}(0)=\tfrac{1}{2},\quad G_{MS}(0)=\tfrac{1}{2}(\mu_p+\mu_n),\quad C_E(0)=1,$$
$$C_Q(0)=M_d{}^2Q,\quad C_S(0)=1-\tfrac{3}{2}P_D,$$

and

$$C_L(0)=\tfrac{3}{2}P_D,$$

where Q is the quadrupole moment of the deuteron, μ_p and μ_n are the proton and neutron magnetic moments, and $P_D=\int_0^\infty W^2(r)dr$ is the D-state probability of the deuteron.

C. Meson-Exchange-Current Corrections

The possibility of contributions to the deuteron current from meson-exchange currents has been discussed by several authors.[22,24–26,33] From considerations of the isotopic spin of the deuteron and the charge conjugation number of the photon exchanged between the electron and deuteron, it is concluded that there must be an odd number of pions in the exchange current. Contributions to the meson-current interaction arising from $\rho\gamma\pi$ coupling have been calculated by Adler and Drell.[24,25] This calculation was made using the impulse approximation and assumptions about the couplings of mesons and nucleons. The results are expressed as additive corrections to the deuteron form factors given by

$$\Delta G_0{}^{\text{meson}}(q)=-(8/3)\eta C'I_1(q),$$
$$\Delta G_1{}^{\text{meson}}(q)=(M_d/M_p)CI_1(q),$$
$$\Delta G_2{}^{\text{meson}}(q)=\frac{3}{2\sqrt{2}}\left[\left(2\sqrt{\frac{8}{9}}\right)C'I_1(q)+C'I_2(q)+CI_3(q)\right],$$

where[34] $I_1(q)$, $I_2(q)$, and $I_3(q)$ are integrals that depend on the deuteron wave functions, and the constants C and C' are related to coupling constants and are given by

$$C=-3Gg_{\rho\gamma\pi}a/16m_\rho e,\quad C'=-3Gg_{\rho\gamma\pi}b/16m_\rho e,$$

where $G^2/4\pi=14$ is the pion-nucleon coupling constant, $e^2/4\pi=1/137$ is the electron-photon coupling constant, m_ρ is the mass of the ρ meson, $g_{\rho\gamma\pi}$ is the ρ-γ-π coupling constant, and $a=G_{EV}(0)=\frac{1}{2}$ and $b=G_{MV}(0)=2.35$ are the ρ-nucleon coupling constants. The constant $g_{\rho\gamma\pi}$ is related to the width $\Gamma_{\rho\gamma\pi}$ for the decay of the ρ meson into a pion and a photon by[35]

$$\Gamma_{\rho\gamma\pi}=\frac{1}{24}\frac{g_{\rho\gamma\pi}{}^2}{4\pi}m_\rho\left(1-\frac{m_\pi{}^2}{m_\rho{}^2}\right)^3.$$

D. Relativistic Corrections

A number of attempts have been made to derive a relativistic theory for elastic e-d scattering. Dispersion-theory treatments[36–40] have usually been limited to low values of q^2. The most complete calculation of relativistic effects in the elastic e-d cross section has been made by Gross.[27] The corrections are of two types, arising from the expansion of the nucleon current to order M^{-2} and the treatment of the deuteron wave function in a relativistic manner so as to retain terms of order M^{-2} which describe the distortion of the wave function of a moving deuteron. The form factors with relativistic corrections can be written

$$G_0=(1+\eta)^{-1/2}\{G_{ES}C_E+G_{ES}I_C+(2G_{MS}-G_{ES})J_C\},$$
$$G_2=(1+\eta)^{-1/2}\{G_{ES}C_Q+G_{ES}I_Q+(2G_{MS}-G_{ES})J_Q\},$$
$$G_1=\frac{(1+\tfrac{1}{2}\eta)G_{ES}-3\eta(G_{ES}-G_{MS})}{(1+\eta)^{1/2}}C_L+\frac{2(1+\tfrac{1}{2}\eta)}{(1+\eta)^{1/2}}G_{MS}C_S+\frac{2}{(1+\eta)^{1/2}}[G_{ES}I_{M1}+G_{MS}(I_{M2}+J_{M1})+(G_{ES}-G_{MS})J_{M2}].$$

[33] D. R. Harrington, Phys. Rev. **133B**, 142 (1964).

[34] We have used the formulas of R. J. Adler, [Ph.D. thesis Stanford University, 1965 (unpublished)] which had been reduced to a form suitable for computer calculation by E. F. Erickson [Ph.D. thesis, Stanford University, 1965 (unpublished)].

[35] S. Berman and S. Drell, Phys. Rev. **133B**, 791 (1964).

[36] H. F. Jones, Nuovo Cimento **26**, 790 (1962); **27**, 1039(E) (1963).

[37] F. Gross, Phys. Rev. **134B**, 405 (1965); **136B**, 140 (1964).

[38] K. Deitz and M. Month, Phys. Rev. **152**, 1364 (1966).

[39] R. J. Adler and E. F. Erickson, Nuovo Cimento **40B**, 236 (1965).

[40] M. Gourdin, M. Le Bellac, F. M. Renard, and J. Tran Thanh Van, Nuovo Cimento **37**, 524 (1964).

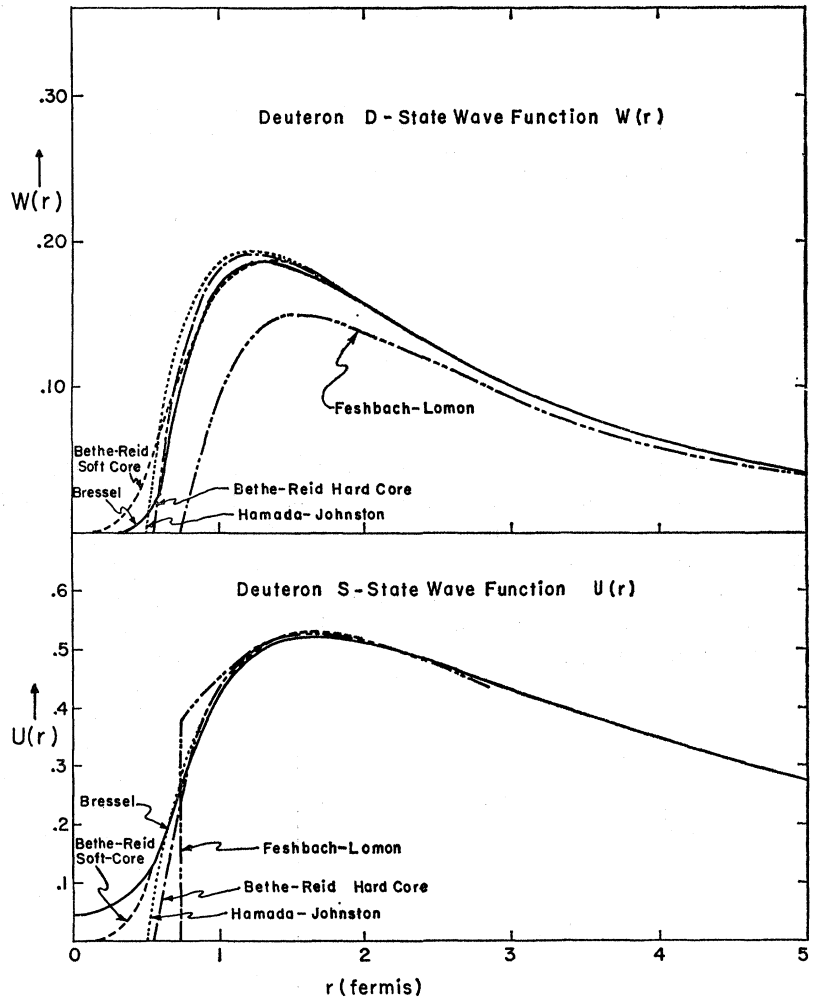

FIG. 5. Various deuteron wave functions. The S- and D-state wave functions, $U(r)$ and $W(r)$, respectively, of Bressel, Feshbach, and Lomon, Bethe and Reid, Hamada and Johnston, and Hulthén are illustrated. The units of $U(r)$ and $W(r)$ are F^{-2}. We have been informed by A. Kerman that an error has been found in the short-range behavior of the Bressel wave function. This error is not expected to modify significantly the form factor prediction; however, this matter is now being investigated.

The expressions for the functions of q^2 designated by I_C, J_C, I_Q, J_Q, I_{M1}, I_{M2}, J_{M1}, and J_{M2} involve integrals over nonrelativistic deuteron wave functions and are given in Ref. 27.

E. Deuteron Wave Functions

The nonrelativistic deuteron wave functions that are used in the prediction of the form factors originate from solutions of the Schrödinger equation for the two-nucleon problem using various proposed nucleon interaction potentials. The free parameters in the various potentials have been optimized by comparing the theoretical predictions of nucleon-nucleon scattering with experimental measurements.

We have computed theoretical deuteron form factors using the wave functions of Hamada and Johnston,[41] Bressel,[42] Feshbach and Lomon,[43] Bethe and Reid,[44] and Hulthén.[45] Some of these are illustrated in Fig. 5, and the static properties of the deuteron predicted from these wave functions are listed in Table V. The Hamada-Johnston potential contains central, tensor, linear, and quadratic L-S terms, and has a hard-core radius of 0.485 F in all states. The Feshbach-Lomon potential employs a boundary condition[46] at 0.73 F and is a modified version of an earlier model.[47] The Bressel potential is similar to the Hamada-Johnston potential but contains a soft core instead of an infinitely repulsive core. The models of Bethe and Reid are also similar to Hamada-Johnston; one potential having a hard core, the other a soft core. The predictions of three Hulthén wave functions, one with no core and the others with hard cores, were included in our comparisons to illustrate the reliability of simple analytic wave functions.

The contributions to $A(q^2)$ from the three deuteron

[41] T. Hamada and I. D. Johnston, Nucl. Phys. **34**, 382 (1962).

[42] C. N. Bressel, Ph.D. thesis, Massachusetts Institute of Technology, 1965 (unpublished). See the caption to Fig. 5 for a remark concerning these results.

[43] H. Feshbach and E. Lomon (private communication); Rev. Mod. Phys. **39**, 611 (1967).

[44] H. Bethe and R. V. Reid, Jr., (private communication); and R. V. Reid, Jr., MIT-LNS Report, 1968 (unpublished).

[45] L. Hulthén and M. Sugawara, in *Handbüch der Physik*, edited by S. Flügge (Springer-Verlag, Berlin, 1957), Vol. 39, p. 1.

[46] H. Feshbach and E. Lomon, Ann. Phys. (N. Y.) **29**, 19 (1964).

[47] H. Feshbach, E. Lomon, and A. Tubis, Phys. Rev. Letters **6**, 635 (1961); **7**, 39(E) (1962).

TABLE V. Properties of various nucleon-nucleon interaction potentials.

Potential	Percent D state	Predicted magnetic dipole moment	Predicted quadrupole moment (F)^2	Core or boundary condition radius (F)
Hamada-Johnston	6.96	0.840	0.281	0.485
Bressel	6.49	0.842	0.281	0.686
Feshbach-Lomon	4.31	0.854	0.268	0.734
Bethe-Reid (hard core)	6.50	0.842	0.277	0.548
Bethe-Reid (soft core)	6.47	0.842	0.280	0.057
Hulthén (no core)	4.00	0.856	0.271	0.000
Hulthén	4.00	0.856	0.271	0.432
Hulthén	4.00	0.856	0.271	0.561
Experimental	...	0.85741±0.00008	0.282±0.002	...

form factors based on the wave functions of Hamada and Johnston are illustrated in Fig. 6 to show the general features of their results. The charge form factor dominates the theoretical predictions for low q^2, and the quadrupole part dominates in the region of the node in the charge form factor. Values of the integrals used are listed in Table VI for reference.

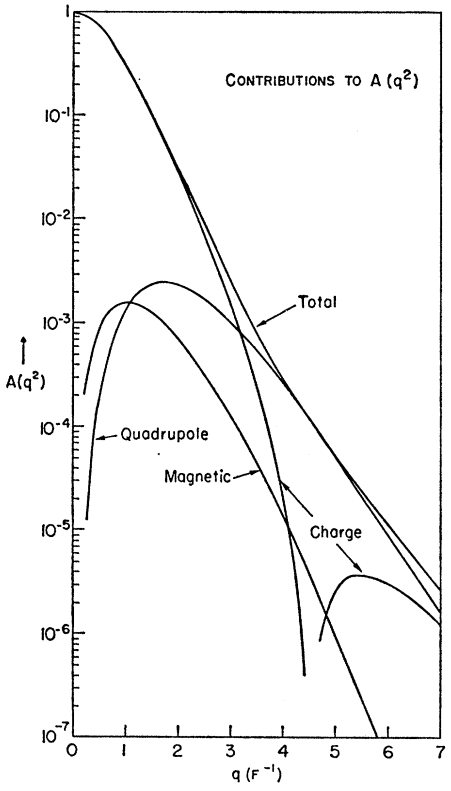

FIG. 6. Contributions to $A(q^2)$ from terms involving the charge, quadrupole moment, and magnetic moment form factors of the deuteron. The contributions correspond to the terms $G_0^2(q^2)$, $(8/9)\eta^2 G_2(q^2)$, and $\frac{2}{3}\eta G_1^2(q^2)$, respectively. The Hamada-Johnston wave function was used in these predictions. See also the caption to Fig. 4.

V. COMPARISON OF EXPERIMENT WITH THEORETICAL MODELS

An important objective of this experiment was to investigate the relative success of wave functions obtained from various nucleon-nucleon potential models in predicting the elastic e-d scattering cross section at large momentum transfers. The theoretical evaluations used in these comparisons are limited by uncertainties arising from experimental errors in the values of the nucleon form factors, from relativistic corrections, and from meson-exchange-current contributions.

The errors in the prediction of $A(q^2)$ arising from the errors in the nucleon form factors were estimated by fitting smooth curves to the measurements of these quantities and determining the uncertainty in the curves

TABLE VI. Values of integrals calculated using Hamada-Johnston wave functions. The integrals are used in predicting $A(q^2)$.

q (F^{-1})	$C_E(q)$	$C_Q(q)$	$C_S(q)$	$C_L(q)$
0.00	1.00×10^{0}	2.54×10^{1}	8.96×10^{-1}	1.04×10^{-1}
0.25	9.62×10^{-1}	2.47	8.61	1.03
0.50	8.63	2.22	7.71	1.01
0.75	7.37	1.91	6.57	9.69×10^{-2}
1.00	6.11	1.58	5.45	9.18
1.25	4.98	1.29	4.46	8.60
1.50	4.01	1.05	3.62	7.98
1.75	3.19	8.55×10^{0}	2.92	7.35
2.0	2.53	6.94	2.36	6.72
2.25	1.98	5.64	1.90	6.11
2.50	1.53	4.59	1.53	5.53
2.75	1.17	3.75	1.22	4.97
3.00	8.73×10^{-2}	3.07	9.78×10^{-2}	4.46
3.25	6.35	2.52	7.79	3.99
3.50	4.44	2.07	6.17	3.55
3.75	2.92	1.70	4.86	3.14
4.00	1.71	1.41	3.79	2.78
4.25	7.48×10^{-3}	1.16	2.91	2.44
4.50	6.65×10^{-5}	9.63×10^{-1}	2.21	2.15
4.75	-5.56×10^{-3}	7.99	1.65	1.88
5.00	−9.80	6.63	1.20	1.64
5.25	-1.29×10^{-2}	5.51	8.30×10^{-3}	1.42
5.50	−1.51	4.57	5.39	1.22
5.75	−1.65	3.80	3.14	1.06
6.00	−1.73	3.15	1.38	9.10×10^{-3}
6.25	−1.76	2.62	-4.20×10^{-6}	7.70
6.50	−1.76	2.18	-1.05×10^{-3}	6.43

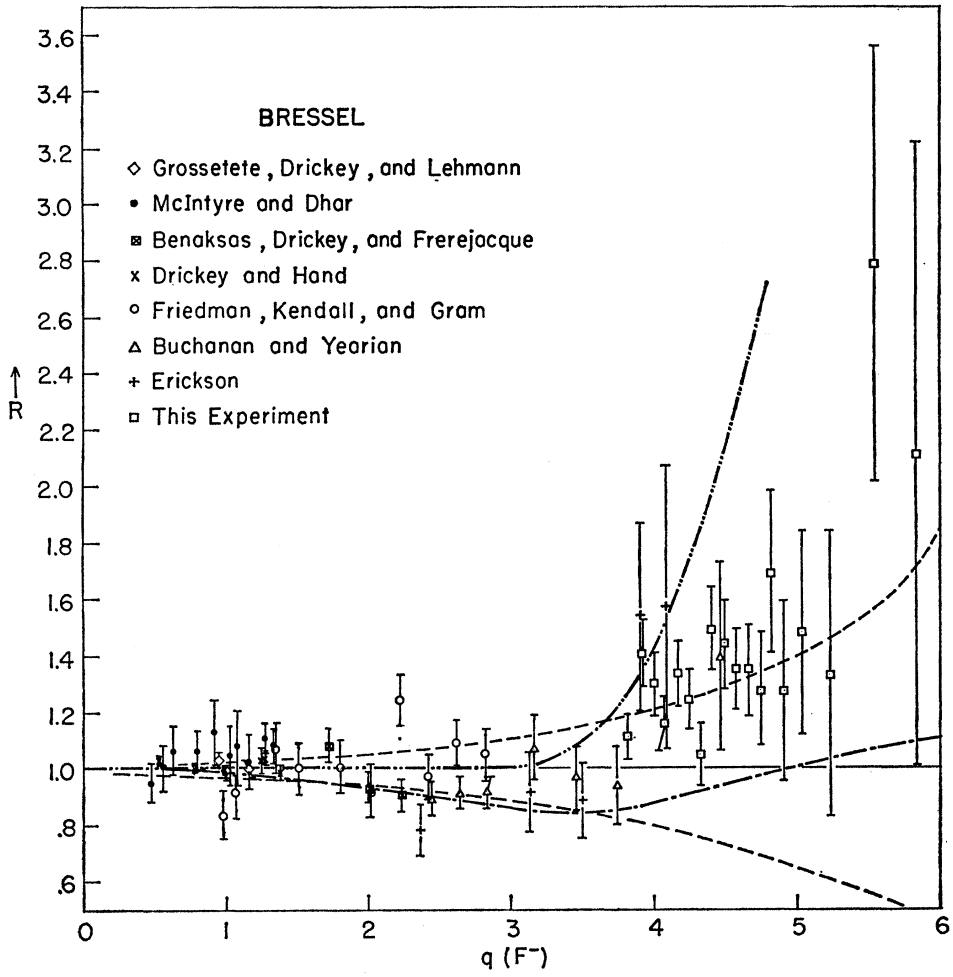

FIG. 7. Ratio R of the experimental measurements of $A(q^2)$ to the theoretical predictions using the wave functions of Bressel. The theoretical predictions do not include meson exchange or relativistic corrections. The latter effects are indicated by showing the ratio of the corrected to the uncorrected theory. The dash-double-dot curve includes the meson exchange corrections. The dash-dot curve includes the relativistic corrections. A ρ-γ-π coupling constant corresponding to a width of 0.5 MeV was used in the predictions of the meson-exchange correction. The dashed band indicates a 1-standard-deviation uncertainty in G_{ES}^2 arising from the errors in the parameters of the fit to the nucleon form-factor data.

according to statistical theory. The fits, which employed both dipole and two-pole forms, were intended to provide a method of interpolating between the experimental measurements. The fits to $G_{ES}(q^2)$ used measurements[20,48] of $G_{Ep}(q^2)$ over a range of q^2 from 0 to 45 F^{-2} combined with measurements[49–51] of $G_{En}(q^2)$ derived from inelastic e-d scattering. The errors of $G_{ES}(q^2)$ included both the errors of the measurements of $G_{Ep}^2(q^2)$ and $G_{En}^2(q^2)$. The values of $G_{En}(q^2)$ were set equal to zero, since measurements of $G_{En}^2(q^2)$ are negative or zero. The fit to $G_{MS}(q^2)$ used measurements[20,48,52,53] of $G_{Mp}(q^2)$ combined with measurements[49–51,54–56] of $G_{Mn}(q^2)$. The dipole fits gave values within the predicted error band of the two-pole fit. The fits and associated error bands were consistent with the fits of deVries *et al.*[54] Since $A(q^2)$ depends strongly on $G_{ES}(q^2)=\frac{1}{2}[G_{ES}(q^2)+G_{En}(q^2)]$, the values of $G_{En}(q^2)$ are important at large q^2. To allow for possible oscillations in the value of $G_{En}(q^2)$, such as have been investigated by Chilton and Uhrhane[57] on the basis of dispersion calculations, we have increased the error band of $G_{ES}(q^2)$ by adding the statistical error in quadrature with an amount proportional to the amplitude of the oscillations that they estimate. Their results give values of $G_{En}(q^2)$ which are consistent with the experimental values of $G_{En}(q^2)$ obtained from elastic e-d scattering at low values of q^2, with values obtained from inelastic e-d scattering at high values of q^2, and with the nonzero slope of $G_{En}(q^2)$ at $q^2=0$. The dashed bands in

[48] W. Bartel, B. Dudelzak, H. Krehbial, J. M. McElroy, U. Meyer-Berkout, R. J. Morrison, H. Nguyen-Ngoc, W. Schmidt, and G. Weber, Phys. Rev. Letters **17**, 608 (1966).

[49] E. B. Hughes, T. A. Griffy, M. R. Yearian, and R. Hofstadter, Phys. Rev. **139B**, 458 (1965).

[50] J. R. Dunning, Jr., K. W. Chen, A. A. Cone, G. Hartwig, N. F. Ramsey, J. K. Walker, and Richard Wilson, Phys. Rev. **141**, 1286 (1966).

[51] P. Stein, M. Binkley, R. McAllister, A. Suvi, and W. Woodward, Phys. Rev. Letters **16**, 592 (1966).

[52] We used the data of F. Bumiller and R. Hofstadter and of P. A. M. Gram and E. Dally as analyzed by L. N. Hand, D. G. Miller, and R. Wilson, Rev. Mod. Phys. **35**, 335 (1963).

[53] B. Dudelzak, Ph.D. thesis, University of Paris, 1965 (unpublished).

[54] C. deVries, R. Hofstadter, A. Johansson, and R. Herman, Phys. Rev. **134B**, 848 (1964), as analyzed by Hand, Miller, and Wilson; see Ref. 53.

[55] B. Grossetête, S. Jullian, and P. Lehmann, Phys. Rev. **141**, 1435 (1966).

[56] C. W. Akerlof, K. Berkelman, G. Rouse, and M. Tigner, Phys. Rev. **135B**, 810 (1964).

[57] F. Chilton and F. J. Uhrhane (to be published).

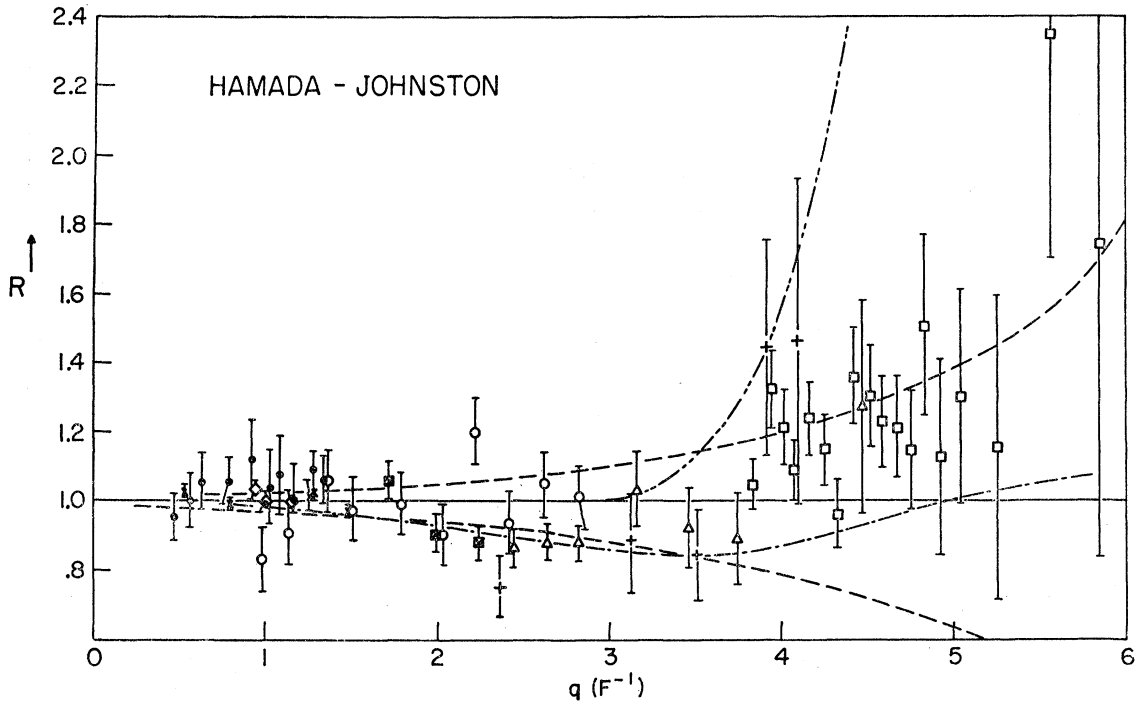

FIG. 8. Ratios of the experimental measurements of $A(q^2)$ to the theoretical predictions using the wave functions of Hamada and Johnston. See caption to Fig. 7.

Figs. 7–11 illustrate the error band finally obtained. This error band allows $G_{En}(q^2)$ to be roughly one-third of $G_{Ep}(q^2)$ at $q^2=36$ F^{-2}.

In Figs. 7–11 are plotted the ratios of the experimental measurements to the theoretical predictions using the formulas of Sec. IV B, and various wave functions. Also shown in these figures are the effects of relativistic corrections[58] and meson-exchange-current corrections. The value of the $\rho\gamma\pi$ coupling constant we used corresponds to $\Gamma_{\rho\gamma\pi}=0.5$ MeV. An upper limit on the value of $\Gamma_{\rho\gamma\pi}$ of 0.6 MeV with 97% confidence has been determined experimentally by a direct measurement of $\rho\rightarrow\gamma\pi$.[59] Values of 0.19 and 0.45 MeV have been obtained by fitting various models to measurements of ρ photoproduction.[60] A value of 0.055 ± 0.04 MeV has been inferred using the Berman-Drell model[35] relating ρ and ω photoproduction and a measurement of $\Gamma_{\omega\gamma\pi}$.[60] Using SU(6) unitary-symmetry schemes which predict $\Gamma_{\rho\gamma\pi}=\frac{1}{9}\Gamma_{\omega\gamma\pi}$,[61] one finds $\Gamma_{\rho\gamma\pi}=0.07\pm0.03$ MeV. Thus it follows that 0.5 MeV represents a reasonable upper limit on $\Gamma_{\rho\gamma\pi}$, and that $\Gamma_{\rho\gamma\pi}$ may be smaller by a factor of 10. The prediction of the meson-exchange-current correction for values of $\Gamma_{\rho\gamma\pi}$ other than 0.5 MeV can be made by scaling the values given here since the correction is proportional to $\sqrt{(\Gamma_{\rho\gamma\pi})}$. For comparison, we give values of $\Gamma_{\rho\gamma\pi}$ determined by normalizing the theoretical prediction of static magnetic moment to the experimental value using various wave functions. These are 0.99 MeV for Hamada-Johnston, 1.72 MeV for Bressel, and 0.09 MeV for Feshbach-Lomon.

In Table VII are given values of χ^2 computed from a comparison of theory and experiment. The estimates of the uncertainties in $G_{ES}^2(q)$ were included with the errors of the measurements of $A(q^2)$ in the computation of χ^2. The lowest value of χ^2 was obtained using the Hamada-Johnston wave function with neither relativistic nor meson-current corrections. However, the inclusion of the relativistic correction does not seriously worsen the fit and, in general, the relativistic corrections appear to be consistent with the data when used in conjunction with the Hamada-Johnston and Bethe-Reid functions. The values obtained using the Bressel and the two Bethe-Reid wave functions are almost equivalent to the Hamada-Johnston value. Predictions based on the Feshbach-Lomon wave functions without meson-exchange-current corrections fit the data well for values of q^2 less than about 12 F^{-2}, but fall below the data and outside of the error band of $G_{ES}^2(q^2)$ at larger values of q^2. A more conservative estimate of the error band of

[58] The relativistic corrections were computed from Partovi wave functions, which are essentially Hamada-Johnston wave functions, by Dr. E. F. Erickson. We are indebted to Dr. Erickson for providing his computations.

[59] G. Fidecaro, J. A. Poirier, and P. Schiavon, Phys. Letters **23**, 163 (1966).

[60] Aachen-Berlin-Bonn-Hamburg-Heidelberg-München Collaboration, DESY Report 66-32, 1966 (unpublished). See also *Proceedings of the Thirteenth International Conference on High Energy Physics* (University of California Press, Berkeley, 1967), p. 166.

[61] S. Badier and C. Bouchiat, Phys. Letters **15**, 96 (1965); S. L. Glashow and R. H. Socolow, Phys. Rev. Letters **15**, 329 (1965).

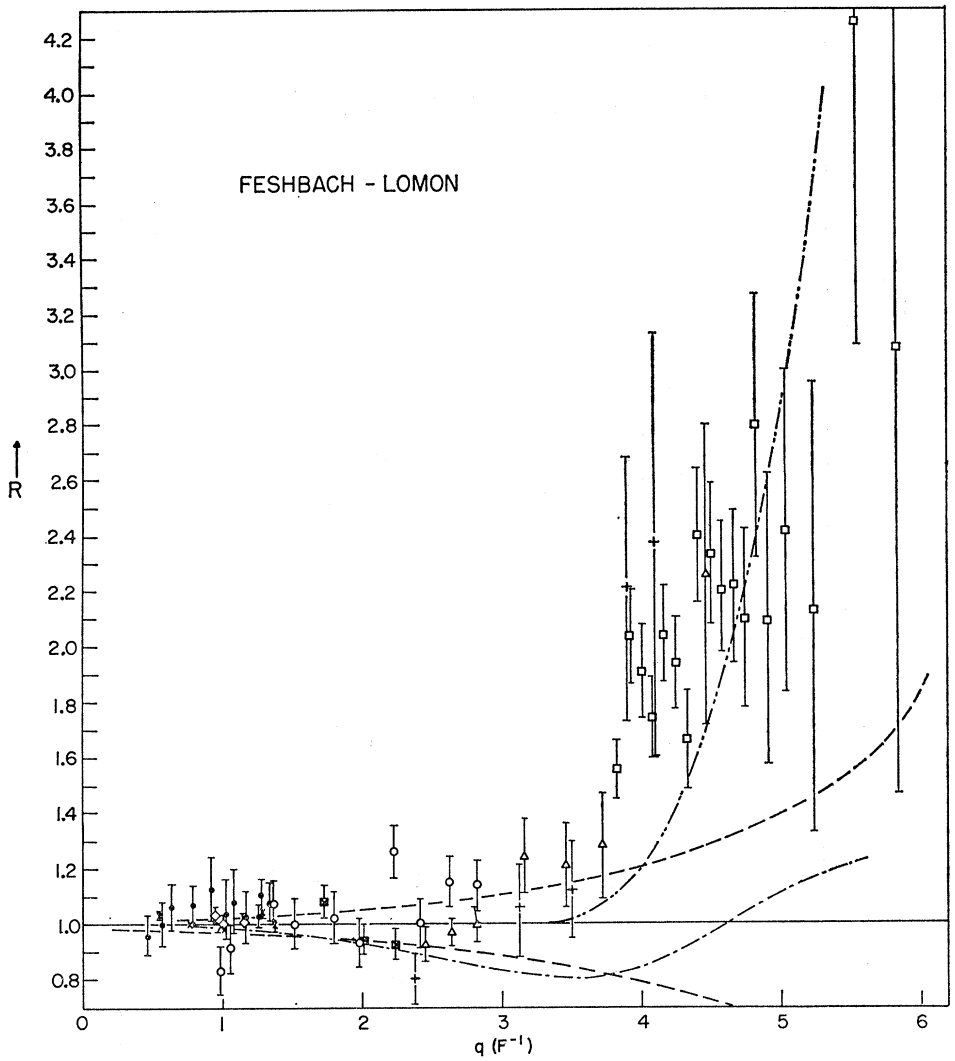

FIG. 9. Ratios of the experimental measurements of $A(q^2)$ to the theoretical predictions using the wave functions of Feshbach and Lomon. See caption to Fig. 7.

$G_{ES}^2(q^2)$ corresponding to the amplitude of the errors of the measurements of $G_{ES}^2(q^2)$ and which ignores plausible theoretical models for $G_{ES}(q^2)$ causes the Feshbach-Lomon predictions and the measurements of $A(q^2)$ to overlap at large values of q^2.

The magnitude of the meson-exchange-current correction required to bring the theory into agreement with the experimental points for values of q^2 greater than about 16 F^{-2} is very dependent on the choice of deuteron wave function. The required meson-exchange contribution needed using the wave functions of Hamada-Johnston, Bressel, and Bethe-Reid is small and consistent with zero considering the magnitude of the uncertainty in $G_{ES}(q^2)$. The Feshbach-Lomon wave function requires a meson-exchange-current correction but with a different momentum dependence. The requirements on the magnitude of the required meson-exchange-current corrections are reversed at $q^2=0$ since the Feshbach-Lomon wave function predicts approximately the correct static magnetic moment, while the predictions of the other wave functions require roughly a 3% correction. An additional form factor, for which there appears some possibility, in the description of the intermediate state in the Adler-Drell model of the meson-current correction would make consistent the $q^2=0$ and large-q^2 behavior of the meson-current corrections required by the Hamada-Johnston, Bressel, and Bethe-Reid wave functions.

Analysis of experiments[7,9] measuring the magnetic form factor of the deuteron using Partovi wave functions, which give predictions almost identical to those of Hamada-Johnston, have shown that the experimental measurements are larger than the theoretical prediction with no meson-exchange-current contribution included. The excess has been attributed to meson-exchange effects and is consistent with predictions of this effect using $\Gamma_{\rho\gamma\pi}=0.5$ MeV. The analysis in this paper indicates that the experimental measurements of the charge and quadrupole moment form factors are consistent with the theoretical predictions using Hamada-Johnston

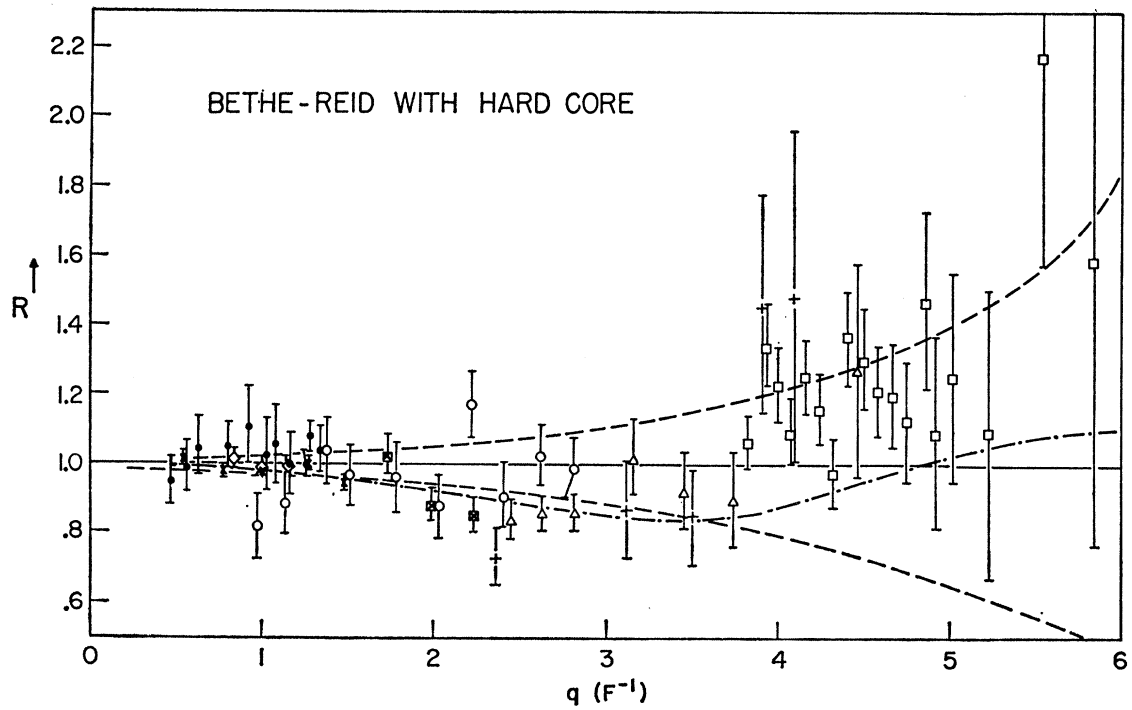

FIG. 10. Ratios of the experimental measurements of $A(q^2)$ to the theoretical predictions using the wave functions from the hard-core model of the Bethe and Reid. See caption to Fig. 7.

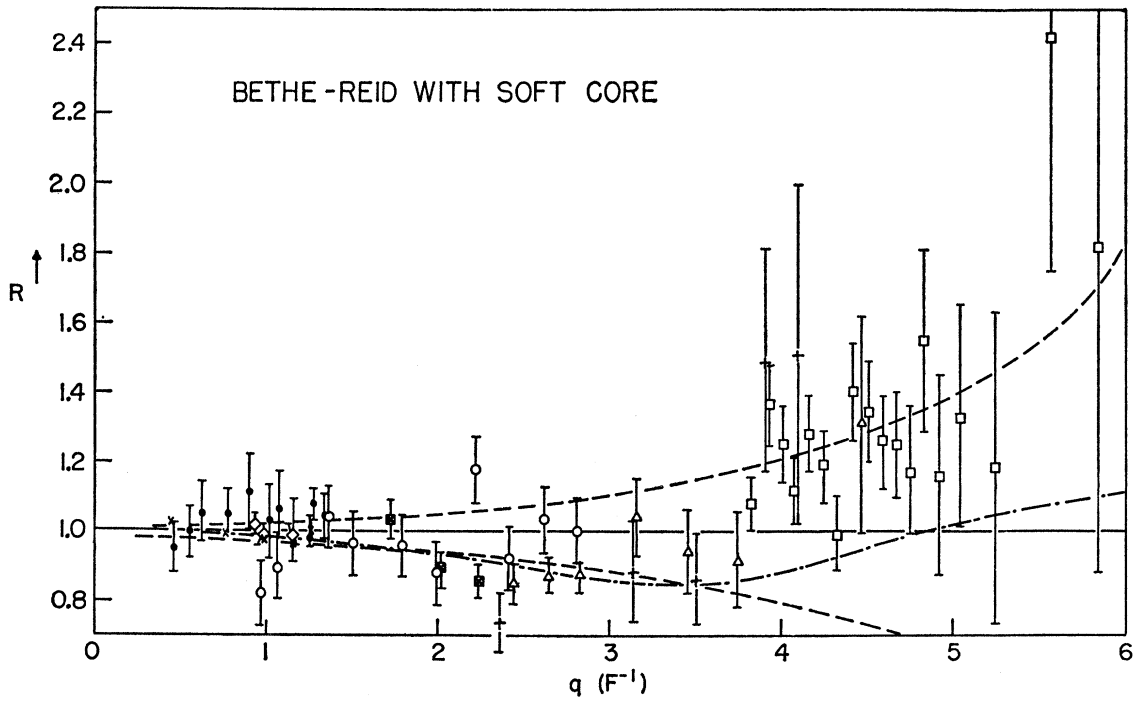

FIG. 11. Ratios of the experimental measurements of $A(q^2)$ to the theoretical predictions using the wave functions from the soft-core model of Bethe and Reid. See caption to Fig. 7.

wave functions without meson-exchange-current contributions.

The behavior of form factors of bound composite systems at large values of q^2 has been investigated by Drell *et al.*[62] They used the Schrödinger equation to examine how the radial dependence of the two-nucleon-

[62] S. D. Drell, A. C. Finn, and Michael H. Goldhaber, Phys. Rev. 157, 1402 (1967).

TABLE VII. Values of χ^2 from a comparison of theory and experiment.[a]

Theory	χ^2 over the range of q (F^{-1}) from 0–1	1–2	2–3	3–4	4–5	5–6	Total χ^2	Total χ^2 for theory with relativistic corrections
Bressel	10.9	15.1	18.1	6.8	18.5	4.4	73.8	103.5
Hamada-Johnston	10.9	11.8	24.7	6.1	10.5	3.0	67.1	77.5
Feshbach-Lomon	10.9	15.4	15.7	25.6	79.7	9.1	156.4	212.1
Bethe-Reid (hard core)	11.3	10.7	32.3	6.4	10.8	2.5	73.9	71.9
Bethe-Reid (soft core)	11.3	10.9	30.7	6.4	12.9	3.3	75.4	75.4
Hulthén (core, 0.561 F)	11.1	12.5	18.7	48.6	111.3	9.8	212.0	257.2
Hulthén (core, 0.432 F)	11.5	11.2	24.7	26.6	102.1	12.2	188.2	226.2
Hulthén (no core)	14.7	40.6	409.0	171.7	35.9	3.3	675.3	324.3
Number of measurements	9	16	11	8	14	4	62	62

[a] Values of χ^2 for ranges of q are given for the theory without relativistic or meson-exchange corrections. The uncertainties in $G_{ES}^2(q^2)$ were included with the experimental errors of $A(q^2)$ in the computations of χ^2.

interaction potential influences the form factor. In particular, they were interested in the effects of a realistic hard core in the interaction. They used a model of the radial dependence of a repulsive-core potential which is proportional to $(r_0/r)^{2(1+p)}$, where r_0 is a scaling factor and p is a parameter greater than zero. The asymptotic form factor predicted from this interaction has been compared with our experimental values of $A(q^2)/G_{ES}^2(q^2)$ in the range of q^2 from 4 to 35 F^{-2}. The comparison indicates that the best fit occurs for $p<0.09$ and $r_0<0.002$ F, which is an unreasonably small value. However, further investigation is required to determine whether the kinematic range of this experiment allows the form factor to reach a sufficiently asymptotic value to provide a valid comparison with this theoretical point of view.

VI. SUMMARY AND CONCLUSIONS

In the present experiment we have made measurements of a combination of the charge and electric quadrupole form factor of the deuteron over a range of q^2 from 14.4 to 35.4 F^{-2}. The deuteron was momentum-analyzed and identified by ionization and range measurements and detected in coincidence with the scattered electron. These measurements extended the range of q^2 from a maximum value of 20 F^{-2} that had previously been reached. Detailed comparisons of the experimental measurements of the deuteron form factor were made with theoretical predictions based on various deuteron wave functions. The theoretical predictions included estimates of relativistic and meson-exchange-current corrections. To estimate the uncertainty in the theoretical predictions due to the experimental uncertainty of $G_{ES}=\frac{1}{2}(G_{Ep}+G_{En})$, fits were made to the nucleon form-factor measurements. The measurements of G_{En} were taken from inelastic e-d scattering experiments. The uncertainties in the fits were added in quadrature to a theoretical estimate of possible nonzero values of G_{En}. In this way an estimate of the theoretical uncertainties in the nucleon form factor models was included.

Good agreement was obtained between this experiment and a theory without meson-exchange corrections and using the deuteron wave functions of Hamada-Johnston, Bressel, and the hard- and soft-core models of Bethe-Reid. The prediction of the Feshbach-Lomon wave function is systematically below the data at high values of q^2 without additional corrections put into the theory. The meson-exchange-current correction required by the Hamada-Johnston, Bressel, and Bethe-Reid wave functions to give agreement with this experiment is considerably smaller than that required in predicting the magnetic form factor of the deuteron as indicated by the latest measurements of the deuteron magnetic form factor. The Feshbach-Lomon wave function appears to require larger meson-exchange-current contributions at high values of q^2, but with a different dependence on q^2. The relativistic corrections of Gross when used with the Hamada-Johnston and Bethe-Reid wave functions appear to be consistent with the experimental data. More detailed conclusions about the meson-exchange-current and relativistic corrections cannot be made at present owing both to the model dependence of the deuteron wave functions and to the experimental errors of the nucleon isotopic scalar form factor. The uncertainties in the measurements of the nucleon isotopic form factor make a major contribution to the uncertainties in the interpretation of our results. More accurate measurements of the charge form factor of the neutron would narrow considerably the number of deuteron wave functions whose predictions fit the measurements of the deuteron form factor.

ACKNOWLEDGMENTS

We are indebted to the staff of the Cambridge Electron Accelerator for their support during the preparation and running of this experiment. The willing help of the members of the staff of the Laboratory for Nuclear Science at M.I.T. is gratefully acknowledged, and, in particular, we wish to thank Dr. Fred Eppling and Professor Peter Demos for their continuing support. We wish to thank Dr. R. Smith and Professor R.

Alvarez, who contributed to the early stages of the experiment. The assistance of Professor Richard Wilson and members of his group was essential and is gratefully acknowledged. Professor E. Lomon, Professor H. Feshbach, and Dr. R. V. Reid kindly provided us with deuteron wave functions, and we thank Dr. E. F. Erickson, who furnished calculations of the relativistic corrections. The assistance of D. Freeman and Mrs. J. Miller with many computational problems is greatly appreciated.

PHYSICAL REVIEW VOLUME 177, NUMBER 5 25 JANUARY 1969

Double Regge Description of ω Production in K^+p Interactions*

G. ALEXANDER, A. FIRESTONE, C. FU, G. GOLDHABER, AND A. PIGNOTTI†
Department of Physics and Lawrence Radiation Laboratory, University of California, Berkeley, California 94720
(Received 20 September 1968)

We present results on the ω and φ production in $K^+p \to K^+\omega p$ and $K^+p \to K^+\varphi p$ interactions at incident momenta of 4.6 and 9.0 GeV/c. There is no statistically significant evidence for $K\omega$ or $K\varphi$ resonance production. The 437 $K^+\omega p$ events at 9 GeV/c are analyzed in terms of a multiperipheral Regge model on the entire Dalitz plot. The events have been assigned to the various peripheral diagrams on the basis of criteria in the four-momentum transfers. A satisfactory description of the data has been obtained on the basis of diagrams involving Pomeranchuk and meson exchanges.

I. INTRODUCTION

In the past, the Regge-pole model, which has been relatively successful in describing high-energy two- and quasi-two-body reactions, has been extended to multiparticle reactions.[1] In particular, there have been some recent applications of the multiperipheral Regge-pole model to three-body final state reactions.[2–4] Because the Regge model was originally introduced as an asymptotic expansion, in these works the model was used to fit only the comparatively small fraction of events for which all two-particle subenergies were larger than some prescribed values. In the case of the reactions $\pi p \to \rho\pi p$, Berger[5] succeeded in extending the model down to threshold in the $\pi\rho$ subenergy, but was forced to perform a cut in the πN mass to avoid the strong presence of the Δ resonance. Here we deal with the process $K^+p \to K^+\omega p$ in which no strong resonances are observed, and we attempt a fit over the entire Dalitz plot with a double Regge model. A justification of this attempt may be found in the proposed extension of the Dolen-Horn-Schmid duality argument,[6] according to which the multi-Regge formalism describes not only the asymptotic behavior of the production amplitude, but also its behavior at lower energies, in some average sense. If strong resonances are present, we cannot expect this average description to be a precise one; on the other hand, if no resonant effects are observed, it is tempting to try a detailed fit over the entire Dalitz plot.

In this work we have studied the production of ω and φ mesons in K^+p interactions at 4.6 and 9.0 GeV/c in the final-state configurations $K^+\omega p$ and $K^+\varphi p$. We attempt to describe in detail only the more abundant $K^+\omega p$ channel at 9 GeV/c in terms of the multiperipheral Regge-pole model.

In Sec. II we describe the experimental procedure and results. In Sec. III we summarize the multiperipheral formalism used in this work, and in Sec. IV we discuss its application to the $K^+p \to K^+\omega p$ data at 9 GeV/c.

II. EXPERIMENTAL RESULTS

The experiment was carried out with pictures taken in the 80-in. hydrogen bubble chamber at the Brookhaven National Laboratory alternating gradient synchrotron, exposed to an rf-separated K^+ beam. Some 50 000 pictures were taken with an incident K^+ beam momentum of 4.6 GeV/c and some 90 000 pictures with an incident momentum of 9 GeV/c. The four-prong events were measured with the LRL Flying-Spot Digitizer and the remeasurements were carried out with a conventional digitizing machine. The events were then spatially reconstructed and kinematically

* Work supported by the U. S. Atomic Energy Commission.
† Present address: Department of Physics, University of California at Santa Barbara, Goleda, Calif.
[1] T. W. B. Kibble, Phys. Rev. **131**, 2282 (1963); K. A. Ter-Martirosyan, Zh. Eksperim. i Teor. Fiz. 44, 341 (1963) [English transl.: Soviet Phys.—JETP **17**, 233 (1963)].
[2] Chan Hong-Mo, K. Kajantie, and G. Ranft, Nuovo Cimento **49A**, 157 (1967); Chan Hong-Mo, K. Kajantie, G. Ranft, W. Beusch, and E. Flaminio, *ibid.* **51A**, 696 (1967).
[3] E. L. Berger, Phys. Rev. Letters **21**, 701 (1968).
[4] S. Ratti, in Topical Conference on High Energy Collisions of Hadrons, CERN, Geneva, January 1968, Vol. I, p. 611 (unpublished).
[5] E. L. Berger, Phys. Rev. **166**, 1525 (1968).
[6] R. Dolen, D. Horn, and C. Schmid, Phys. Rev. **166**, 1768 (1968); G. F. Chew and A. Pignotti, Phys. Rev. Letters **20**, 1078 (1968).